GeoPlanning
Journal of Geomatics and Planning

Geoplanning: Journal of Geomatics and Planning, Vol. 12, No. 1, 2025, 15 - 30

e-ISSN: 2355-6544

Received: 09 September 2024;
Revised: 08 May 2025;
Accepted: 09 May 2025;
Available Online: 14 May 2025;
Published: 26 May 2025.

Keywords:
Urbanization, Coastal Metropolitan, Data Fusion, Obia

*Corresponding author(s)
email: abdurrahman.zaki20@pwk.undip.ac.id

Original Research Open access

Coastal Metropolitan Dynamics in Poland's Tri-City and Indonesia's Semarang: NTL, BLFEI, and OBIA in Google Earth Engine

Abdurrahman Zaki[1*], Joanna Jaskuła[1]

1. *Faculty of Environmental and Mechanical Engineering, Poznań University of Life Sciences, Poland*

DOI: 10.14710/geoplanning.12.1.15-30

Abstract

The increasing global urbanization, particularly in coastal regions, coupled with the risks of climate change and land subsidence, underscores the need to monitor coastal urban development for sustainability. This study focused on the coastal metropolitan regions of Poland's Tri-City and Indonesia's Semarang, employing GIS, remote sensing (RS), and cloud computing. By integrating nighttime light (NTL) and the Built-Up Land Features Extraction Index (BLFEI) through Google Earth Engine (GEE) and Object-Based Image Analysis (OBIA), the study aimed to gain insights into urban development trends. The methodology encompassed image collection, analysis, and classification over three decades (1992, 2007, 2022). Despite efforts to enhance accuracy through built-up masking in subsequent years, the methodology achieved an overall accuracy of 95% for the 2022 maps, while maps in 1992 and 2007 fell short (overall accuracy ranging from 0.81 to 0.90) in comparison. The analysis revealed a gradual expansion of built-up areas in both regions, with Gdynia and Gdańsk emerging as primary drivers in the Tri-City metropolitan region and Semarang as the primary driver in the Semarang metropolitan region. Notably, the Semarang metropolitan region exhibited an increase in waterbody areas, attributed to coastal flooding and land subsidence challenges.

1. Introduction

The world's population is projected to reach between 9.4 to 10.1 billion by 2050 and between 9.4 to 12.7 billion by 2100, according to the United Nations (2019a). By 2050, more than 68% of the global population is expected to reside in cities due to urbanization (United Nations, 2019b). In many developing countries, urbanization often occurs without proper planning (Gumel et al., 2020; Sun et al., 2020), resulting in unsustainable urban development (Clement & Pino, 2023; Das et al., 2021; Esther, 2022). Ultimately, the impacts of urbanization in developing countries could be more severe than those in developed countries (Ezadin & Faraj, 2022).

Factors contributing to urban sprawl in developing countries include increasing population, industrialization (Hasnine & Rukhsana, 2020), the service industry, and real estate development (Zhang & Pan, 2021), as well as peri-urban and infrastructure development (Ahmed et al., 2021). To address sustainable urban development in the future, monitoring the temporal and spatial patterns of urban areas is crucial (Dadashpoor et al., 2019b; Sumari et al., 2019). However, despite the challenges, cities located along coastal areas are still highly preferred residential areas for urban dwellers (Sanders & Oliveira, 2020; Siegel, 2020; Wang et al., 2021).

The future sustainability of coastal cities is threatened by the increasing risks of climate change (Sanders & Oliveira, 2020; Wojtowicz-Jankowska & Kalfouni, 2022), particularly in those located in low-income countries (Day et al. 2021). These coastal cities are at risk of land subsidence (Cian et al., 2019; Hu et al., 2019; Wdowinski et al., 2020), sea level rise (Qu et al., 2019; Taherkhani et al., 2020; Valente & Veloso-Gomes, 2020), rising temperatures (Hu, 2021; Qi et al., 2022), and pollution (Choi et al., 2020; Su et al., 2020). To address these issues, adaptation measures to combat climate change, such as adaptive coastal planning (Valente & Veloso-Gomes, 2020; Buchori et al., 2022) and community-based adaptation (Berman et al., 2020), are needed to prepare for the uncertainties facing coastal cities in the future. In this regard, providing data on changing landscape trends in coastal areas can serve as a monitoring measure and input for coastal adaptation strategies (Hu et al., 2021; Ragia & Krassakis, 2019; Vitousek et al., 2023).

The monitoring of temporal and spatial changes in the Earth's landscape across vast areas is commonly carried out using a geographic information system (GIS) and remote sensing (Buchori et al., 2015; Fahad et al., 2020; Liu & Yang, 2015; Woodcock et al., 2020; Zhang, 2020). Previous studies have demonstrated that GIS and remote sensing can be effectively used to analyze historical land use and land cover (LULC) maps (Adnani et al., 2019; Viana et al., 2019), predict future LULC maps using the Cellular Automate (CA) algorithm (Hishe et al. 2020; Mathanraj et al., 2021; Muhammad et al., 2022), and even apply object-based image analysis (OBIA) for improved accuracy in classifying LULC maps (How et al., 2020; Pangastuti & Wijayanto, 2021; Yadav et al., 2022; Zaki et al., 2022). Recently, cloud computing, particularly Google Earth Engine, has significantly accelerated image analysis, enabling scholars to analyze large areas at the national or global scale without consuming local computer memory (Luo et al., 2021; Yadav et al., 2022; Zaki et al., 2022; Zaki et al., 2023; Zhang & Li, 2022).

When classifying Land Use and Land Cover (LULC) maps, a persistent issue is the occurrence of the "salt and pepper effect," which refers to the scattering of misclassified pixels. This phenomenon is particularly noticeable when using pixel-based image analysis, a conventional method for image classification. To mitigate the salt and pepper effect, a more recent classification method known as Object-Based Image Analysis (OBIA) was developed. OBIA functions by segmenting pixels before the classification process, allowing for the merging of scattered pixels with their homogeneous surrounding environment. In addition to advancing classification methods, efforts to enhance the accuracy of LULC maps have been made through data fusion, which involves the combination of satellite data from various sources to achieve improved results. For instance, prior studies have attempted to fuse Landsat image collections with nighttime light datasets using Google Earth Engine (Goldblatt et al., 2018; Liu et al., 2019). Our primary hypothesis centers on the idea that by integrating OBIA with data fusion, incorporating not only nighttime light data but also a remote sensing index, a scholar can enhance the accuracy of LULC mapping on a broader scale within the framework of Google Earth Engine. A secondary hypothesis aims to demonstrate that urban sprawl is more pronounced in the Semarang metropolitan region (Indonesia) compared to the Tri-City metropolitan region (Poland).

Therefore, the objective of this study is to improve the classification of LULC maps by fusing Landsat image collections, integrating nighttime light (NTL) data, and Built-Up Land Features Extraction Index (BLFEI). This approach enables the analysis of three decades of urban development in medium-sized coastal metropolitan regions in Indonesia and Poland. However, it is essential to acknowledge certain limitations in this study: 1) social and political factors are not considered in this research, and 2) the categorization of LULC classes is limited to built-up areas, non-built-up areas, and waterbodies. Ultimately, this study aspires to contribute to the body of knowledge in GIS and remote sensing methodology for monitoring urban sprawl, thereby promoting sustainable coastal urban development.

2. Data and Methods

2.1. Study Area

The study area of this research includes the coastal areas of the Tri-City metropolitan region in Poland (Figure 1) and the Semarang metropolitan region in Indonesia (Figure 2). These study areas were selected

because they are medium-sized metropolitan cities in their respective countries. In general, the study area was defined as a 20-kilometer radius from the coastal areas of the Tri-City and Semarang metropolitan regions. This definition was chosen considering that administrative boundaries do not limit urban growth, and a broader study area is necessary to encompass the urban core and suburban areas in each region. A radius of 20 kilometers was deemed appropriate to cover these aspects in both metropolitan regions. Additionally, the study area includes water bodies to account for landscape changes such as land reclamation, harbor construction, and coastal erosion.

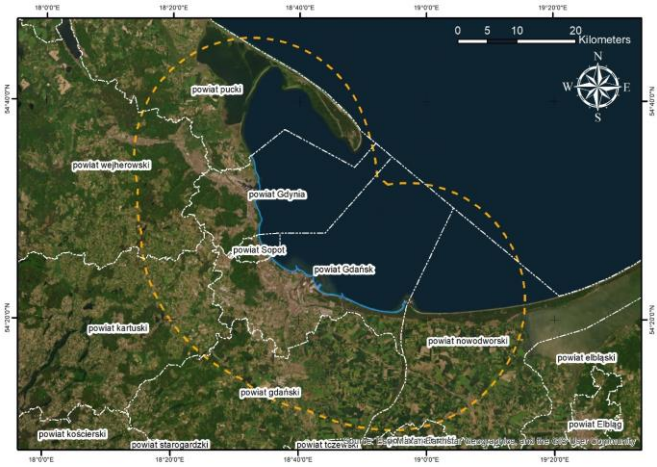

Figure 1. The study area of the Tri-City metropolitan region in Poland

Figure 2. The Study Area of the Semarang Metropolitan Region in Indonesia

2.2. Data

The aim of this research is to monitor urban development over an extended period, and Landsat image collections were chosen as the dataset due to their continuous operation since the 1970s, despite differences between each Landsat mission. Although Sentinel-2A satellite image collections were available, they were not utilized in this research as their operational period only started from June 23, 2015. Instead, Landsat 5 (operational from March 1, 1984, to June 5, 2013; LANDSAT/LT05/C02/T1_L2) and Landsat 8 (operational from February 11, 2013; LANDSAT/LC08/C02/T1_L2) provided by the U.S. Geological Survey (USGS) were used in this study. By utilizing these two Landsat datasets, which consist of atmospherically corrected surface reflectance, the research generated maps for three time periods: 1992, 2007, and 2022. The selection of these years was based on available data, taking into account cloud covers and the availability of nighttime light data.

The next dataset was the nighttime light data, which indicates urbanization. It included the datasets NOAA/DMSP-OLS/NIGHTTIME_LIGHTS with a spatial resolution of 927.67 meters, covering the period from 1992 to 2014, and NOAA/VIIRS/DNB/MONTHLY_V1/VCMSLCFG with a spatial resolution of 463.83 meters, spanning from 2014 to 2023 in Google Earth Engine. This dataset was provided by the Earth Observation Group (Payne Institute for Public Policy, Colorado School of Mines).

The final dataset comprised a set of randomly selected sample points for both built-up and non-built-up areas within each study area for each observation year (1992, 2007, and 2022), as presented in Table 1 and spatially visualized in Figure 3. The process of selecting sample points involved gradually adding samples until the resulting land cover map accurately represented the actual Earth conditions, as observed from natural color Landsat imagery. These sample points were then divided into two sets: 70% for training purposes and 30% for testing (Abdi 2020; Chenli Liu et al. 2020). This division was achieved using the randomColumn() and filter() functions. The training points were utilized for image classification, while the testing points were used to assess the accuracy of the image classification results.

Table 1. Numbers of Sample Points for Built-Up (BU) and Non-Built-Up (NBU) Areas in each region

Year	Tri-City		Semarang	
	BU	NBU	BU	NBU
2022	179	582	368	550
2007	240	268	218	218
1992	192	157	283	127

To be noted, the number of training samples from 2022 to 1992 decreased due to smaller areas to be classified. This reduction was made taking into consideration the possibility that misclassification could result in a built-up area in a previous year that does not exist in the following year. To anticipate this, the area was limited that would be classified using the boundary of classified built-up areas in the following year of observation. However, the downside is that the number of training samples was up to hundreds, making it not time-efficient for purposes requiring fast processing.

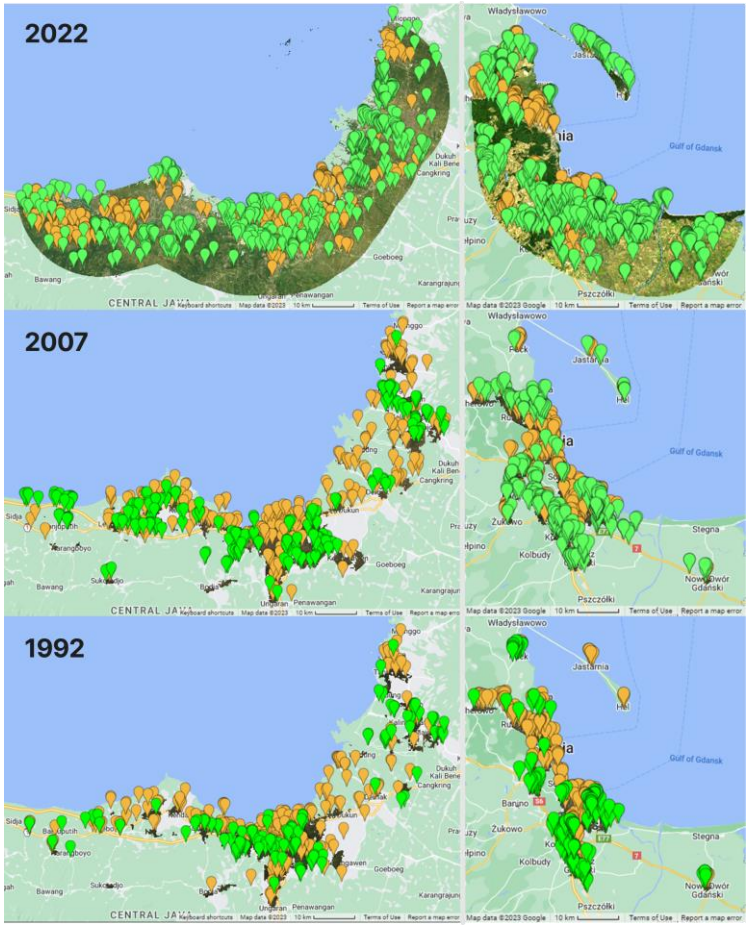

Figure 3. Spatial Distribution of Training Samples in Each Study Area
(Left: Semarang Metropolitan Region; Right: Tri-City Metropolitan Region)

2.3. Methods

This section describes the methodology used in this study, which generally includes initial image processing (filtering and masking), data fusion, and object-based image classification (OBIA). The methodology was predominantly implemented using Google Earth Engine (https://code.earthengine.google.com/), and QGIS Desktop 3.32.1 (https://qgis.org/) for the map layouting. The workflow of this methodology is depicted

in Figure 4. The final output of this process comprises land cover maps delineating built-up areas, non-built-up areas, and water bodies within the two study regions for the years 1992, 2007, and 2022.

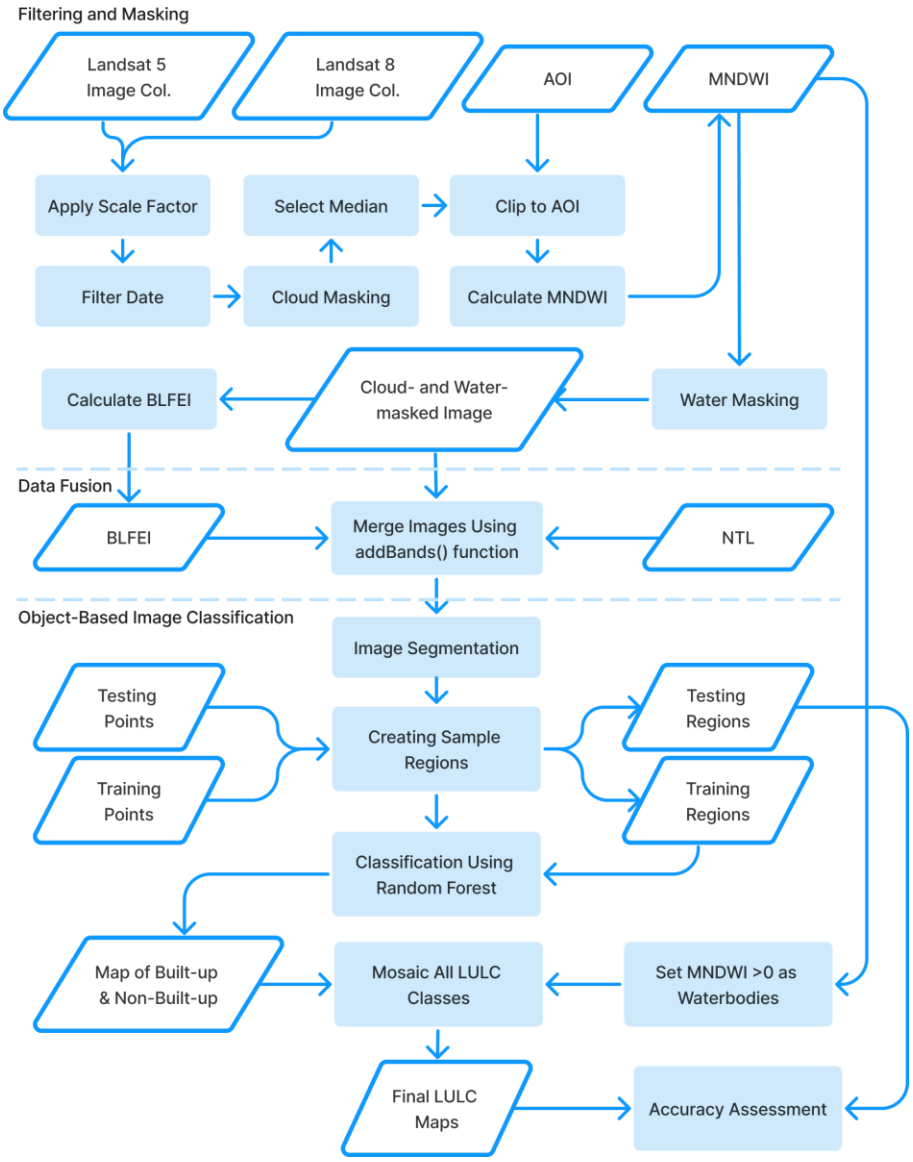

Figure 4. Methodological Workflow Implemented in Google Earth Engine

2.3.1. Initial Image Processing

The processes in the initial phase of the methodology involved filtering the Landsat image collections, applying a scale factor for both Landsat 5 and Landsat 8, performing cloud masking, and subsequently applying water masking using MNDWI (Modified Normalized Difference Water Index). Initially, the filter date selection for both locations (Tri-City and Semarang) took into account when both locations are in the summer/dry season. For example, it was referenced in a previous study that indicated the dry season in the Java province (where the Semarang metropolitan region is located) spans from June to September, with the peak of rainfall in December and January (Berliana et al., 2021). On the other hand, another study mentioned that Torun (a city located 185 kilometers south of the Tri-City) experiences spring from April to October (Kejna & Pospieszyńska, 2023). In this case, the analyzed period was utilized from April 1st to October 31st for each observation year in both locations to filter the Landsat images. Secondly, before using the LANDSAT/LT05/C02/T1_L2 and

LANDSAT/LC08/C02/T1_L2 for calculations, the scale factor must be applied using Equation 1 and Equation 2:

$$optical\ band\ =\ band\ SR\_B \times 0.0000275 + (-0.2) \text{.....(Eq.1)}$$

$$thermal\ band =\ band\ ST\_B \times 0.00341802 +\ 149) \text{.....(Eq.2)}$$

where "band SR_B" refers to all optical bands (B1, B2, B3, B4, B5, B7 in Landsat 5; B1, B2, B3, B4, B5, B6, B7 in Landsat 8), and "band ST_B" refers to" thermal bands (B6 in Landsat 5 and B10 in Landsat 8).

Thirdly, cloud masking was applied to both dataset using the bitmask for the QA_PIXEL band to eliminate clouds, cloud shadows, and snow. The specific bitmask used in this step is detailed in Table 2. This process resulted in image collections with clear terrain. Furthermore, the median value of each pixel was selected, and the image was clipped to the area of interest.

Table 2. Bitmask for QA_PIXEL in Landsat 5 and Landsat 8

Bit	Landsat 5	Landsat 8
1	Dilated Cloud	Dilated Cloud
2	Unused	Cirrus
3	Cloud	Cloud
4	Cloud Shadow	Cloud Shadow
5	Snow	Snow

In the final stage of the initial processing, water masking was executed using MNDWI (see Equation 3), an index proposed by Xu (2006) to identify water bodies, where MNDWI greater than zero indicates water. In this case, MNDWI less than or equal to zero was used to filter the image collections that were previously cloud-masked. The calculation of MNDWI was performed using the Equation 3, where Green and MIR represent band 2 and band 5 in Landsat 5, and band 3 and band 6 in Landsat 8, respectively.

$$MNDWI = \frac{Green-MIR}{Green+MIR}) \text{.....(Eq.3)}$$

2.3.2. Data Fusion

After obtaining the cloud- and water-masked Landsat image collection, the next step was to integrate this collection with nighttime light data and BLFEI. For the nighttime light data, the median values of pixels within the period from January 1st to December 31st were selected and cropped using the boundary of the water-masked image of the study area. However, the datasets used in this step had different spatial resolutions (927.67 meters for NOAA/DMSP-OLS/NIGHTTIME_LIGHTS and 463.83 meters for NOAA/VIIRS/DNB/MONTHLY_V1/VCMSLCFG).

Then, BLFEI proposed by Bouhennache et al. (2019) which resulted in higher accuracy than some other built-up indexes was calculated. The calculation of BLFEI was performed using the Equation 4:

$$BLFEI = \frac{(\frac{Green+Red+SWIR2}{3} - SWIR1)}{(\frac{Green+Red+SWIR2}{3} + SWIR1)} \text{.....(Eq.4)}$$

where the bands used in the formula for Landsat 5 and Landsat 8 were shown in Table 3. Finally, Landsat images, nighttime light images, and BLFEI were combined using the "addBands" function in Google Earth Engine.

Table 3. Bands in Landsat 5 and Landsat 8 used for calculating BLFEI

	Landsat TM		Landsat OLI	
	Band	Wavelength (micrometers)	Band	Wavelength (micrometers)
Green	2	0.52-0.60	3	0.53-0.59
Red	3	0.63-0.69	4	0.64-0.67
SWIR 1	5	1.55-1.75	6	1.57-1.65
SWIR 2	7	2.08-2.35	7	2.11-2.29

Source: https://www.usgs.gov/faqs/what-are-band-designations-landsat-satellites

2.3.3. Object-Based Image Analysis

The final step was to conduct object-based image analysis (OBIA) to monitor urban development patterns. Initially, image segmentation was performed to cluster similar pixels from the result of data fusion into polygons, which is an essential step in OBIA. In this case, it was used a size of 15 and "hex" as the grid type when performing super pixel clustering based on Simple Non-Iterative Clustering (SNIC) in Google Earth Engine. The result of image segmentation is illustrated in Figure 5.

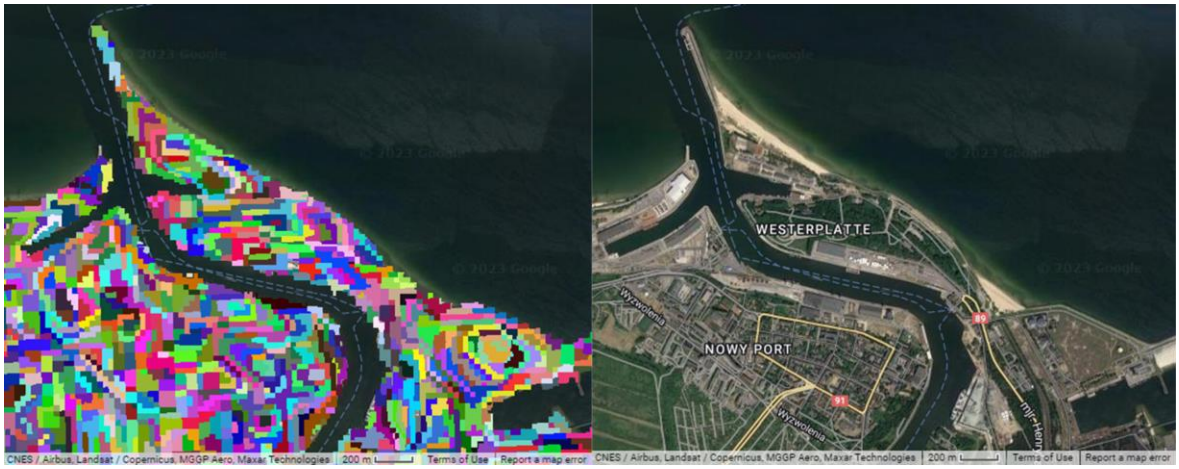

Figure 5. Segmentation result (left) and Google satellite imagery (right) in an area located in the northern Tri-City, Poland

And then, some polygons were selected as training regions based on the previously prepared random training points. Using these training regions, classification using the random forest algorithm was performed to simulate LULC maps. In this case, the number of trees set for the random forest algorithm was 50, referring to Junaid et al., (2023). Since the water bodies were excluded from the initial stage, blank data in the study area was set as water bodies and combined with the resulted LULC from the OBIA. Finally, all results of calculations in Google Earth Engine were exported to Google Drive to be further downloaded, visualized, and analyzed in QGIS Desktop 3.32.1.

3. Result and Discussion

This section comprises a description of the results from the analysis between urban development in the a medium-sized coastal metropolitan region in Poland and Indonesia. The results include interpretations of the data used during the data fusion process, such as Landsat images, the NTL, and the BLFEI. Additionally, there are discussions about the LULC maps resulting from the Object-Based Image Analysis (OBIA) method in Google Earth Engine, representing urban development in both study areas. This section is followed by a discussion of these results in relation to other relevant studies to understand how they correlate with the existing body of knowledge.

3.1. Results

The coastal metropolitan regions exhibited gradual expansion, with green open spaces converted into built-up areas and the construction of toll roads further stimulating rapid urban growth. Overall, the development of built-up areas in both regions aligned with the primary transportation networks connecting other cities. This expansion is illustrated in Figure 6 and Figure 7, which depict each study area using BLFEI and NTL. The data shows a varying range across the years, with the variance in NTL attributed to advancements in satellite technologies that have resulted in higher spatial resolution, particularly noticeable when comparing the 2007 and 2022 data. BLFEI effectively highlights built-up areas through its reddish coloration on the map. Additionally, these maps reveal an expanding coastline in both regions due to harbor development and land reclamation. In the Semarang metropolitan region, however, land subsidence and coastal flooding are particularly pronounced in the northeastern coastal area.

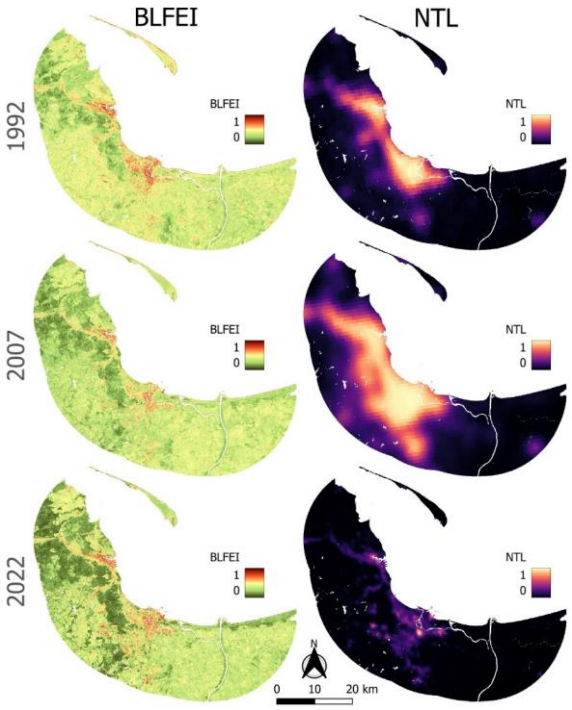

Figure 6. BLFEI and Nighttime Light **Data** in the Tri-City Metropolitan Region

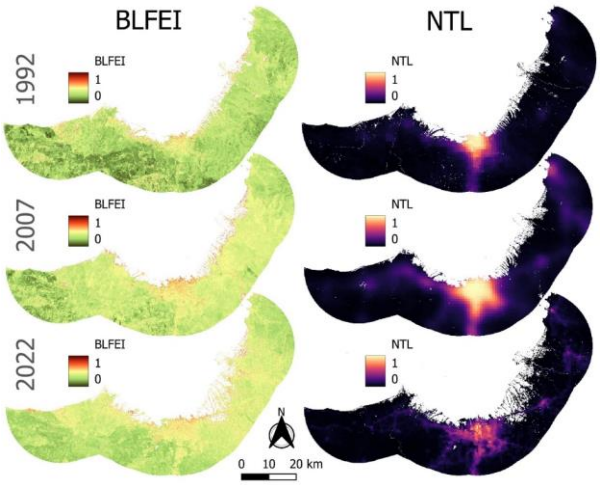

Figure 7. BLFEI and Nighttime Light Data in the Semarang Metropolitan Region

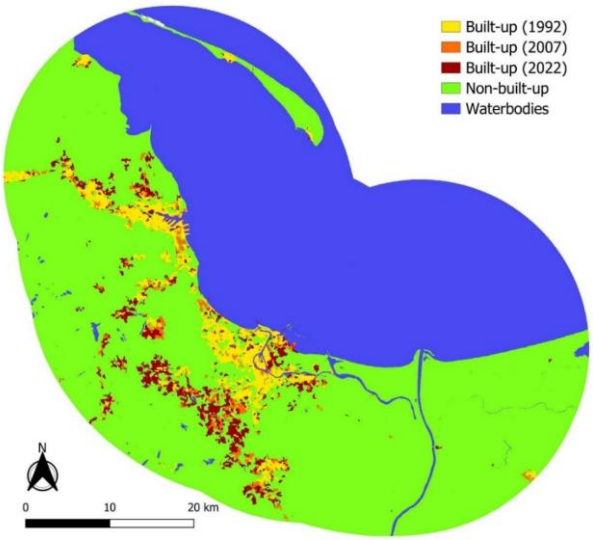

Figure 8. Identification of Built-Up Expansion in the Tri-City Metropolitan Region

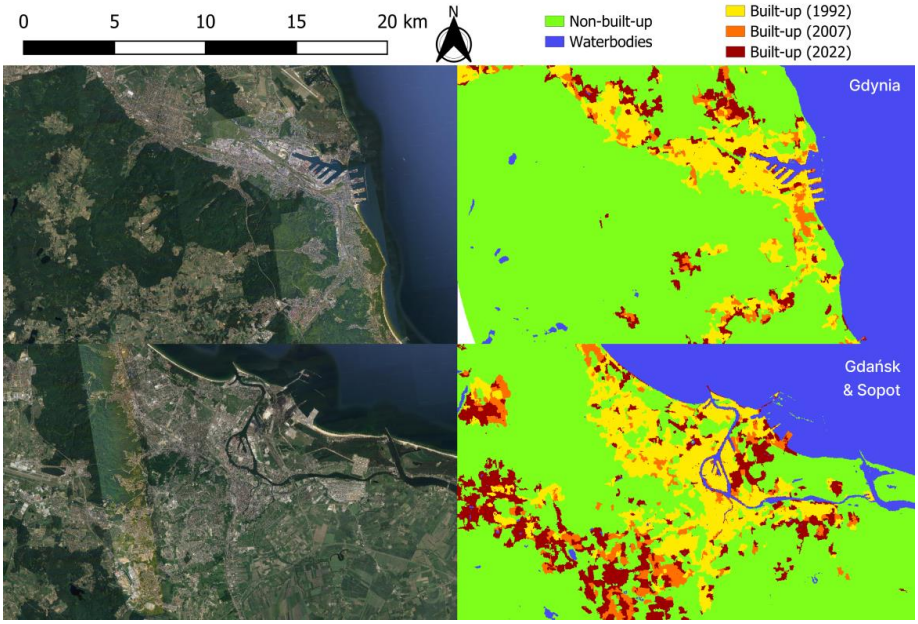

Figure 9. Land Cover Map vs. Google Satellite Image in Tri-City's Cities

Figure 8 and Figure 10, resulting from the application of OBIA to the combination of all Landsat bands, NTL, and BLFEI, illustrate the evolution of built-up areas in both study regions. In the Tri-City metropolitan area, Gdynia and Gdańsk act as primary drivers of urban development, with Sopot serving as a connector between these cities and forming a cohesive metropolitan zone. The presence of harbors in both Gdynia and Gdańsk, along with an international airport in Gdańsk, significantly fuels urban expansion. The dominant housing type in Poland, characterized by numerous apartments and multi-story buildings, contributes to more compact urban development. In contrast, in the Semarang metropolitan region, Semarang city is the main driver of growth, linking neighboring cities such as Kendal, Demak, and Ungaran. The harbor and domestic airport in Semarang also play crucial roles in spurring urban expansion. However, the prevalence of single-family houses in Indonesia, which is more prone to causing urban sprawl, contrasts with the denser housing patterns seen in Poland. Additionally, Figure 9 and Figure 11 provide a detailed comparison between the land cover map and Google satellite images for each city in the study areas.

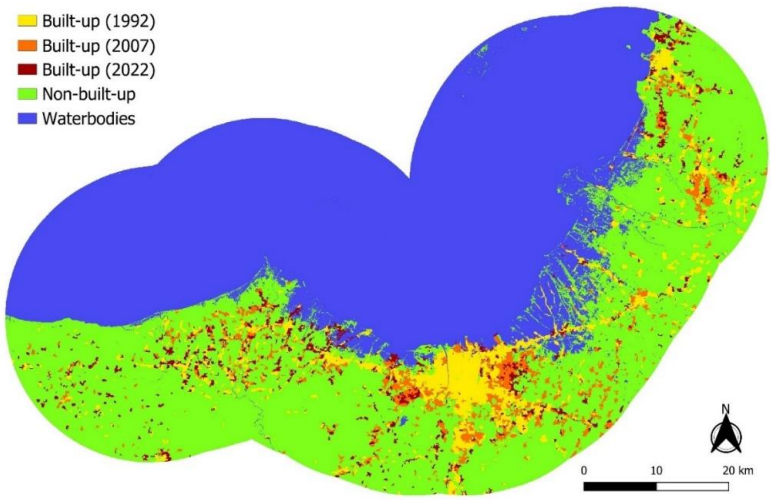

Figure 10. Identification of Built-Up Expansion in the Semarang Metropolitan Region

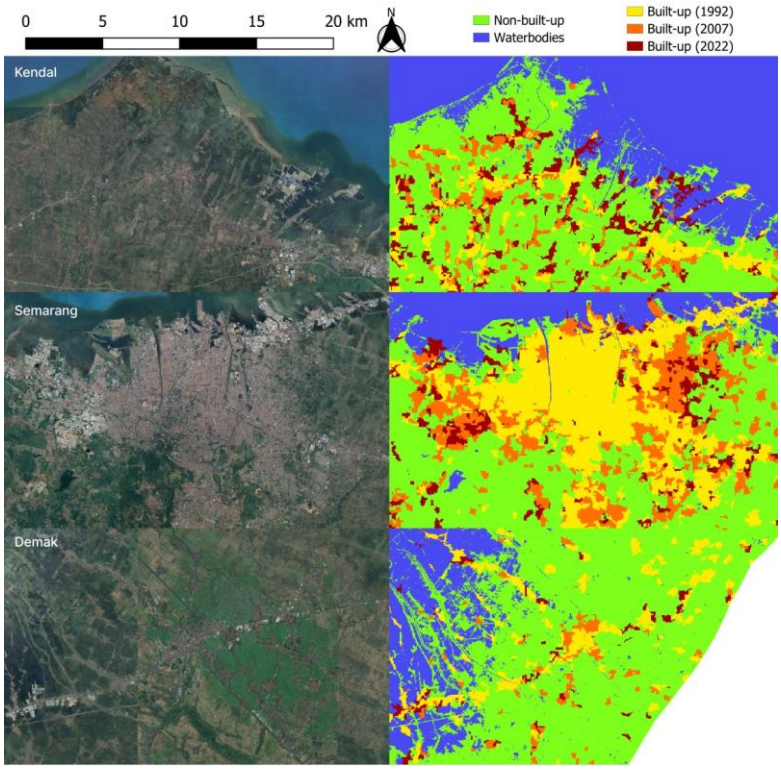

Figure 11. Land Cover Map vs. Google Satellite Image in Semarang

The LULC maps resulting from this study exhibit varied overall accuracy (OA) statistics, following a similar pattern for both study areas: the OA of the subsequent year is higher than that of the preceding year. The methodology achieved an overall accuracy of 95% for the 2022 maps. The OA for the Tri-City metropolitan region in 1992 and 2007 stands at 81% and 87%, respectively, as shown in Table 4. Similarly, for the Semarang metropolitan region, the OA in 1992 and 2007 is 87% and 90%, respectively, presented in Table 5. Despite the expectation to increase the OA of an LULC map by masking it based on the built-up areas in the following year, the accuracy of the LULC maps in 1992 and 2007 still falls short compared to the OA in 2022.

Table 4. Overall Accuracy of Land Cover Maps in the Tri-City Metropolitan Region

	1992		2007		2022	
	BU	**NBU**	**BU**	**NBU**	**BU**	**NBU**
BU	42	5	60	9	43	7
NBU	8	15	5	30	5	173
OA	0.81		0.87		0.95	

Table 5. Overall Accuracy of Land Cover Maps in the Semarang Metropolitan Region

	1992		2007		2022	
	BU	**NBU**	**BU**	**NBU**	**BU**	**NBU**
BU	71	2	62	1	95	5
NBU	9	5	8	18	7	149
OA	0.87		0.90		0.95	

In both study areas, there is a general increase in built-up areas and a decrease in non-built-up areas, as illustrated in Table 6. In the Tri-City region, built-up areas increased by 32.75 square kilometers or 34.45% during 1992-2007 and by 68.88 square kilometers or 53.89% during 2007-2022. Conversely, in Semarang, built-up areas expanded by 142.80 square kilometers or 58.60% in the 1992-2007 period and by 99.31 square kilometers or 25.70% in the 2007-2022 period. This indicates a faster rate of built-up development in the Tri-City region during the 2007-2022 period, while in the Semarang metropolitan region, the acceleration was observed in the 1992-2007 period. However, in the Semarang metropolitan region, there is an increase in the area of waterbodies due to the well-known issues of coastal flooding and land subsidence.

Table 6. Changes in Area for Each Land Cover Class in Both Study Areas

Year	Tri-City			Semarang		
	Built up	Non-Built up	Waterbodies	Built up	Non-Built up	Waterbodies
1992 (km^2)	95.06	1617.52	1303.09	243.69	2172.79	2342.57
2007 (km^2)	127.81	1588.27	1298.84	386.49	2003.31	2369.15
2022 (km^2)	196.69	1520.70	1297.30	485.80	1848.02	2425.29
1992-2007 (Δ)	32.75	-29.25	-4.25	142.80	-169.48	26.58
2007-2022 (Δ)	68.88	-67.57	-1.54	99.31	-155.29	56.14
1992-2007 (%)	34.45	-1.81	-0.33	58.60	-7.80	1.13
2007-2022 (%)	53.89	-4.25	-0.12	25.70	-7.75	2.37

3.2. Discussion

Similar data fusion techniques were employed by Goldblatt et al. (2018) who combined nighttime light data with a Landsat 8 image collection. Using pixel-based image analysis, they achieved accuracies ranging from 80.5% to 87.2% for a nationwide built-up classification. On the other hand, while Liu et al. (2019) were able to produce built-up maps with an overall accuracy of at least 94.7%. Their approach relied on VIIRS nighttime light data, which offers higher spatial resolution and has been available since 2014. This is in contrast to the DMSP-OLS nighttime light data, which was available from 1992 to 2014 and was used for generating the maps in 1992 and 2007 in our research.

Differing from the aforementioned studies, this research employed an Object-Based Image Analysis (OBIA) approach—a method designed to mitigate the salt-and-pepper effect when classifying high-resolution images. It involved the classification of fused images from Landsat, nighttime light data, and BLFEI, resulting in maps with accuracies ranging from 0.81 to 0.95. However, it's important to note that the fusion of these three images did not achieve the expected high accuracy for all years. Notably, it was successful only for the year 2022, despite our efforts to enhance accuracy by incorporating built-up masking from the 2022 map when classifying land covers in 2007 and built-up masking from the 2007 map when classifying land covers in 1992. Nevertheless, the utilization of the OBIA method in Google Earth Engine appeared promising, as it offers a simpler workflow

compared to implementing it in the Orfeo ToolBox (OTB) of the QGIS software, as demonstrated in a previous study (Zaki et al., 2022).

In addition to the accuracy assessment, both the Tri-City and Semarang metropolitan regions have experienced rapid urban expansion, signifying an increase in urban density in the city centers and a sprawling process in their suburban areas. This comparison indicates that the distance between urban centers in a metropolitan region influences the dynamics of urban development. On one hand, the Tri-City metropolitan region comprises Gdańsk and Gdynia, situated only about 22 kilometers apart as two major urban centers in 1992, with Sopot located in between, playing a significant role in driving urban growth. On the other hand, the Semarang metropolitan region primarily relies on Semarang as the sole main driver of urban development within its area. Kendal to the west and Demak to the east serve as neighboring cities, with both cities being approximately 30 kilometers away from Semarang. However, it's worth noting that, in general, urban development in both metropolitan regions follows transportation networks that connect urban centers to surrounding cities. In the case of Semarang, there is a phenomenon known as "desa kota" indicating a blurred distinction between suburban and urban areas (McGee, 2022). This phenomenon has not been observed in the Tri-City metropolitan region.

It is worth noting that coastal urban areas are particularly susceptible to flood risks, especially with the increasing threat of climate change, exacerbated by land subsidence. A previous study analyzed land subsidence occurring in Gdańsk and Gdynia in 2018 and 2020 (Rajaoalison & Knez, 2021). However, based on our observations, the severity of land subsidence in these areas does not appear to be as pronounced as what has been observed on the coast of the Semarang metropolitan region. In the Semarang region, some residents' houses are already experiencing flooding, leading to forced migration or the necessity to raise the height of roads and homes over time (Buchori et al., 2018; Buchori et al., 2021). This trend is evident in the resulting maps from our study, showing that in the eastern part of the Semarang metropolitan region's coast, water bodies have been expanding since 1992 to 2022. In contrast, such a phenomenon has not been observed along the coast of the Tri-City metropolitan region.

The LULC classes employed in this study are limited to three categories: built-up, non-built-up, and waterbodies. Each yearly image resulted from the median value of Landsat images taken between April and October. However, due to variations in the agricultural cycle across years, there are instances when extensive harvested agricultural lands are observed. The fluctuating vegetation patterns throughout the years prompted our focus on a limited range of land cover types, predominantly built-up and non-built-up areas. In future research, conducting a more detailed LULC classification involving categories like bare lands, forest lands, and agricultural lands would facilitate a more comprehensive analysis.

Secondly, green spaces (non-built-up areas) in 2022 were assumed to be the same in 2007 and 1992, implying that there were no afforestation activities within the two study areas. This assumption was made because of observed misclassifications of built-up areas in 2007 and 1992. Therefore, they opted to mask out non-built-up areas in 2022 when classifying land covers in 2007 and to mask out non-built-up areas in 2007 when classifying land covers in 1992. This technique is primarily applicable for classifying land cover changes in developing countries, where it is common for urban areas to continuously expand, and instances of building deconstruction being replaced by vegetation are relatively rare.

Thirdly, the BLFEI and NTL datasets were not normalized before they were merged with the cloud- and water-masked Landsat image collection in the methodology. Consequently, the obtained results suggest that future scholars investigate whether normalization of these two variables could lead to higher accuracy in the final LULC maps. This suggestion is supported by some research demonstrating that normalization positively affected the classification performance using machine learning algorithms (Raju et al., 2020; Singh & Singh, 2020).

Lastly, this research was limited to using the random forest algorithm for LULC classification. However, gaining a deeper understanding of the principles and concepts underlying each machine learning algorithm

would be advantageous for selecting the most suitable algorithm or even testing each to determine the one with the highest accuracy. In the future, exploring the use of the Segment Anything Model (SAM), an artificial intelligence-based image segmentation system developed by Meta AI, could be considered for analyzing urban area maps (Giannakis et al., 2023; Ren et al., 2023; Wang et al., 2023; Zhang et al., 2023). Moreover, future research could perform the projection of future LULC maps; and incorporate 3D building footprint data as it reveals the vertical structure of buildings in urban areas, serving as an additional variable for data fusion.

4. Conclusion

This study attempted to enhance the accuracy of Land Use and Land Cover (LULC) mapping in the coastal areas of metropolitan regions in Indonesia and Poland over three decades (1992, 2007, and 2022). The approach involved data fusion between nighttime light and Landsat image data, along with Object-Based Image Analysis (OBIA), conducted efficiently using the Google Earth Engine cloud computing platform. Despite efforts to improve accuracy through built-up masking in subsequent years, the accuracy assessment of LULC maps revealed varied overall accuracy patterns in both study areas. The methodology achieved an overall accuracy of 95% for the 2022 maps, while maps in 1992 and 2007 fell short (overall accuracy ranging from 0.81 to 0.90) in comparison. Notably, the Semarang metropolitan region exhibited an increase in waterbody areas, attributed to coastal flooding and land subsidence challenges, highlighting the complex dynamics between urbanization and environmental factors.

The analysis uncovered a gradual expansion of built-up areas in both regions, indicating urban development stimulated by primary transportation networks to surrounding cities. In the Tri-City metropolitan area, Gdynia and Gdańsk emerged as primary drivers, with Sopot acting as a crucial connector, forming a cohesive metropolitan zone. The presence of a harbor in Gdynia played a significant role in influencing urban expansion. Conversely, in the Semarang metropolitan region, Semarang city took the lead, linking neighboring cities (Kendal, Demak, Ungaran), with the harbor in Semarang contributing significantly to surrounding urban development. Generally, as a metropolitan region in a developing country, Semarang, with its larger population, has experienced a larger area converted into built-up areas in the same period compared to the more developed Tri-City in Poland.

In conclusion, the study demonstrated a unique approach using OBIA and data fusion, providing insights into urban development dynamics. While successful in 2022, the fusion of images faced challenges in other years. The expansion of water bodies in the Semarang metropolitan region emphasizes the urgency of addressing climate-related risks in coastal urban planning and the need for adaptive strategies.

5. Acknowledgments

The authors would like to thank the editors and reviewers for their valuable comments, which have contributed to improving the quality of the manuscript.

6. References

Abdi, A. M. (2020). Land cover and land use classification performance of machine learning algorithms in a boreal landscape using Sentinel-2 data. *GIScience & Remote Sensing*, *57*(1), 1–20. [Crossref]

Adnani, A. El, Habib, A., Khalidi, K. El, & Zourarah, B. (2019). Spatio-Temporal Dynamics and Evolution of Land Use Land Cover Using Remote Sensing and GIS in Sebou Estuary, Morocco. *Journal of Geographic Information System*, *11*(05), 551–566. [Crossref]

Ahmed, S., Huifang, W., Akhtar, S., Imran, S., Hassan, G., & Wang, C. (2021). An analysis of urban sprawl in Pakistan: consequences, challenges, and the way forward. *International Journal of Agricultural Extension*, *8*(3), 257–278. [Crossref]

Berliana S., S., Susanti, I., Siswanto, B., Nurlatifah, A., Latifah, H., Witono, A., Slamet, L., & Suhermat, M. (2021). Analysis of wet and dry season by using the Palmer Drought Severity Index (PDSI) over Java Island. *The 2nd Science and Mathematics International Conference (SMIC 2020)*, 030010. [Crossref]

Berman, M., Baztan, J., Kofinas, G., Vanderlinden, J.-P., Chouinard, O., Huctin, J.-M., Kane, A., Mazé, C., Nikulkina, I., & Thomson, K. (2020). Adaptation to climate change in coastal communities: findings from seven sites on four continents. *Climatic Change*, *159*(1), 1–16. [Crossref]

Bouhennache, R., Bouden, T., Taleb-Ahmed, A., & Cheddad, A. (2019). A new spectral index for the extraction of built-up land features from Landsat 8 satellite imagery. *Geocarto International*, *34*(14), 1531–1551. [Crossref]

Buchori, I., Pramitasari, A., Pangi, P., Sugiri, A., Maryono, M., Basuki, Y., & Sejati, A. W. (2021). Factors distinguishing the decision to migrate from the flooded and inundated community of Sayung, Demak: A suburban area of Semarang City, Indonesia. *International Journal of Disaster Risk Reduction*, *52*, 101946. [Crossref]

Buchori, I., Sugiri, A., Hadi, S. P., Wadley, D., & Liu, Y. (2015). Developing a geographic information system-based assessment model for sustainable metropolitan development: The case of the Semarang Metropolitan Region, Indonesia. *American Journal of Environmental Sciences*, *11*(2), 62–75. [Crossref]

Buchori, I., Sugiri, A., Mussadun, M., Wadley, D., Liu, Y., Pramitasari, A., & Pamungkas, I. T. D. (2018). A predictive model to assess spatial planning in addressing hydro-meteorological hazards: A case study of Semarang City, Indonesia. *International Journal of Disaster Risk Reduction*, *27*, 415–426. [Crossref]

Buchori, I., Zaki, A., Pangi, P., Sejati, A. W., Pramitasari, A., & Liu, Y. (2022). Adaptation strategies and community participation in government-led mitigation projects: A comparison between urban and suburban communities in Pekalongan, Indonesia. *International Journal of Disaster Risk Reduction*, *81*, 103271. [Crossref]

Choi, J. Y., Jeong, H., Choi, K.-Y., Hong, G. H., Yang, D. B., Kim, K., & Ra, K. (2020). Source identification and implications of heavy metals in urban roads for the coastal pollution in a beach town, Busan, Korea. *Marine Pollution Bulletin*, *161*, 111724. [Crossref]

Cian, F., Blasco, J., & Carrera, L. (2019). Sentinel-1 for Monitoring Land Subsidence of Coastal Cities in Africa Using PSInSAR: A Methodology Based on the Integration of SNAP and StaMPS. *Geosciences*, *9*(3), 124. [Crossref]

Clement, M. T., & Pino, N. W. (2023). Is urbanization sustainable? A longitudinal study of developing nations, 1990-2015. *Environmental Sociology*, *9*(3), 327–347. [Crossref]

Dadashpoor, H., Azizi, P., & Moghadasi, M. (2019). Analyzing spatial patterns, driving forces and predicting future growth scenarios for supporting sustainable urban growth: Evidence from Tabriz metropolitan area, Iran. *Sustainable Cities and Society*, *47*, 101502. [Crossref]

How, J. D., Hasmadi, I. M., & Melissa, M. F. (2020). Assessing Land-Use and Land-Cover Change (LULCC) Between 2009 and 2019 Using Object-Based Image Analysis (OBIA) in Cameron Highlands, Malaysia. In *IOP Conference Series: Earth and Environmental Science* (Vol. 540, No. 1, p. 012002). IOP Publishing. [Crossref]

Das, R. C., Chatterjee, T., & Ivaldi, E. (2021). Sustainability of Urbanization, Non-Agricultural Output and Air Pollution in the World's Top 20 Polluting Countries. *Data*, *6*(6), 65. [Crossref]

Day, J. W., Gunn, J. D., & Burger, J. R. (2021). Diminishing Opportunities for Sustainability of Coastal Cities in the Anthropocene: A Review. *Frontiers in Environmental Science*, *9*. [Crossref]

Esther R., A. (2022). Urbanization and Environmental Unsustainability: An Ecological Footprint Analysis for Nigeria. *African Journal of Environment and Natural Science Research*, *5*(1), 12–24. [Crossref]

Ezadin, N. M., & Faraj, A. (2022). Urbanizatition in Developing Countries. *Journal of Kurdistani for Strategic Studies*, *8*.

Fahad, K. H., Hussein, S., & Dibs, H. (2020). Spatial-Temporal Analysis of Land Use and Land Cover Change Detection Using Remote Sensing and GIS Techniques. *IOP Conference Series: Materials Science and Engineering*, *671*(1), 012046. [Crossref]

Giannakis, I., Bhardwaj, A., Sam, L., & Leontidis, G. (2023). *Deep learning universal crater detection using Segment Anything Model (SAM)*. [Crossref]

Goldblatt, R., Stuhlmacher, M. F., Tellman, B., Clinton, N., Hanson, G., Georgescu, M., Wang, C., Serrano-Candela, F., Khandelwal, A. K., Cheng, W.-H., & Balling, R. C. (2018). Using Landsat and nighttime lights for supervised pixel-based image classification of urban land cover. *Remote Sensing of Environment*, *205*, 253–275. [Crossref]

Gumel, I. A., Aplin, P., Marston, C. G., & Morley, J. (2020). Time-Series Satellite Imagery Demonstrates the Progressive Failure of a City Master Plan to Control Urbanization in Abuja, Nigeria. *Remote Sensing*, *12*(7), 1112. [Crossref]

Hasnine, M., & Rukhsana. (2020). An Analysis of Urban Sprawl and Prediction of Future Urban Town in Urban Area of Developing Nation: Case Study in India. *Journal of the Indian Society of Remote Sensing*, *48*(6), 909–920. [Crossref]

Hishe, S., Bewket, W., Nyssen, J., & Lyimo, J. (2020). Analysing past land use land cover change and CA-Markov-based future modelling in the Middle Suluh Valley, Northern Ethiopia. *Geocarto International*, *35*(3), 225–255. [Crossref]

Hu, B., Chen, J., & Zhang, X. (2019). Monitoring the Land Subsidence Area in a Coastal Urban Area with InSAR and GNSS. *Sensors*, *19*(14), 3181. [Crossref]

Hu, L. (2021). A Global Assessment of Coastal Marine Heatwaves and Their Relation With Coastal Urban Thermal Changes. *Geophysical Research Letters*, *48*(9). [Crossref]

Hu, Y., Yang, C., Yang, J., Li, Y., Jing, W., & Shu, S. (2021). Review on unmanned aerial vehicle remote sensing and its application in coastal ecological environment monitoring. *IOP Conference Series: Earth and Environmental Science*, *821*(1), 012018. [Crossref]

Junaid, M., Sun, J., Iqbal, A., Sohail, M., Zafar, S., & Khan, A. (2023). Mapping LULC Dynamics and Its Potential Implication on Forest Cover in Malam Jabba Region with Landsat Time Series Imagery and Random Forest Classification. *Sustainability*, *15*(3), 1858. [Crossref]

Kejna, M., & Pospieszyńska, A. (2023). Variability in the occurrence of thermal seasons in Poland in 1961–2020. *Meteorological Applications*, *30*(4). [Crossref]

Liu, Chang, Yang, K., Bennett, M. M., Guo, Z., Cheng, L., & Li, M. (2019). Automated Extraction of Built-Up Areas by Fusing VIIRS Nighttime Lights and Landsat-8 Data. *Remote Sensing*, *11*(13), 1571. [Crossref]

Liu, Chenli, Li, W., Zhu, G., Zhou, H., Yan, H., & Xue, P. (2020). Land Use/Land Cover Changes and Their Driving Factors in the Northeastern Tibetan Plateau Based on Geographical Detectors and Google Earth Engine: A Case Study in Gannan Prefecture. *Remote Sensing*, *12*(19), 3139. [Crossref]

Liu, T., & Yang, X. (2015). Monitoring land changes in an urban area using satellite imagery, GIS and landscape metrics. *Applied Geography*, *56*, 42–54. [Crossref]

Luo, J., Ma, X., Chu, Q., Xie, M., & Cao, Y. (2021). Characterizing the Up-To-Date Land-Use and Land-Cover Change in Xiong'an New Area from 2017 to 2020 Using the Multi-Temporal Sentinel-2 Images on Google Earth Engine. *ISPRS International Journal of Geo-Information*, *10*(7), 464. [Crossref]

Mathanraj, S., Rusli, N., & Ling, G. H. T. (2021). Applicability of the CA-Markov Model in Land-use/Land cover Change Prediction for Urban Sprawling in Batticaloa Municipal Council, Sri Lanka. *IOP Conference Series: Earth and Environmental Science*, *620*, 012015. [Crossref]

McGee, T. (2022). Desakota (1991). In *The Horizontal Metropolis* (pp. 393–413). Springer International Publishing. [Crossref]

Muhammad, R., Zhang, W., Abbas, Z., Guo, F., & Gwiazdzinski, L. (2022). Spatiotemporal Change Analysis and Prediction of Future Land Use and Land Cover Changes Using QGIS MOLUSCE Plugin and Remote Sensing Big Data: A Case Study of Linyi, China. *Land*, *11*(3), 419. [Crossref]

Pangastuti, E. I., & Wijayanto, Y. (2021). Land cover analysis using object based image analysis based on Landsat 8 OLI images in the city of Jember. *IOP Conference Series: Earth and Environmental Science*, *747*(1), 012047. [Crossref]

Qi, Y., Li, H., Pang, Z., Gao, W., & Liu, C. (2022). A Case Study of the Relationship Between Vegetation Coverage and Urban Heat Island in a Coastal City by Applying Digital Twins. *Frontiers in Plant Science*, *13*. [Crossref]

Qu, Y., Jevrejeva, S., Jackson, L. P., & Moore, J. C. (2019). Coastal Sea level rise around the China Seas. *Global and Planetary Change*, *172*, 454–463. [Crossref]

Ragia, L., & Krassakis, P. (2019). Monitoring the changes of the coastal areas using remote sensing data and geographic information systems. In G. Papadavid, K. Themistocleous, S. Michaelides, V. Ambrosia, & D. G. Hadjimitsis (Eds.), *Seventh International Conference on Remote Sensing and Geoinformation of the Environment (RSCy2019)* (p. 48). SPIE. [Crossref]

Rajaoalison, H., & Knez, D. (2021). Current trends In land subsidence of the North-Central part of Poland using DInSAR technique. *E3S Web of Conferences*, *266*, 03006. [Crossref]

Raju, V. N. G., Lakshmi, K. P., Jain, V. M., Kalidindi, A., & Padma, V. (2020). Study the Influence of Normalization/Transformation process on the Accuracy of Supervised Classification. *2020 Third International Conference on Smart Systems and Inventive Technology (ICSSIT)*, 729–735. [Crossref]

Ren, S., Luzi, F., Lahrichi, S., Kassaw, K., Collins, L. M., Bradbury, K., & Malof, J. M. (2023). *Segment anything, from space?* [Crossref]

Sanders, F. C., & Oliveira, A. C. de. (2020). Resilience of coastal cities with accumulating climate-change coupled threats; depends on the cooperation of government, experts and the citizens. *IOP Conference Series: Earth and Environmental Science*, *588*(3), 032037. [Crossref]

Siegel, F. R. (2020). *An Example of Coastal Cities Hazard Exposure and Economics* (pp. 63–69). [Crossref]

Singh, D., & Singh, B. (2020). Investigating the impact of data normalization on classification performance. *Applied Soft Computing*, *97*, 105524. [Crossref]

Su, L., Sharp, S. M., Pettigrove, V. J., Craig, N. J., Nan, B., Du, F., & Shi, H. (2020). Superimposed microplastic pollution in a coastal metropolis. *Water Research*, *168*, 115140. [Crossref]

Sumari, N. S., Xu, G., Ujoh, F., Korah, P. I., Ebohon, O. J., & Lyimo, N. N. (2019). A Geospatial Approach to Sustainable Urban Planning: Lessons for Morogoro Municipal Council, Tanzania. *Sustainability*, *11*(22), 6508. [Crossref]

Sun, L., Chen, J., Li, Q., & Huang, D. (2020). Dramatic uneven urbanization of large cities throughout the world in recent decades. *Nature Communications*, *11*(1), 5366. [Crossref]

Taherkhani, M., Vitousek, S., Barnard, P. L., Frazer, N., Anderson, T. R., & Fletcher, C. H. (2020). Sea-level rise exponentially increases coastal flood frequency. *Scientific Reports*, *10*(1), 6466. [Crossref]

United Nations. (2019a). *The world population prospects 2019: highlights*. https://population.un.org/wpp/Publications/Files/WPP2019_Highlights.pdf

United Nations. (2019b). *World Urbanization Prospects: The 2018 Revision (ST/ESA/SER.A/420)*. United Nations. https://www.un.org/development/desa/publications/2018-revision-of-world-urbanization-prospects.html

Valente, S., & Veloso-Gomes, F. (2020). Coastal climate adaptation in port-cities: adaptation deficits, barriers, and challenges ahead. *Journal of Environmental Planning and Management*, *63*(3), 389–414. [Crossref]

Viana, C. M., Girão, I., & Rocha, J. (2019). Long-Term Satellite Image Time-Series for Land Use/Land Cover Change Detection Using Refined Open Source Data in a Rural Region. *Remote Sensing*, *11*(9), 1104. [Crossref]

Vitousek, S., Buscombe, D., Vos, K., Barnard, P. L., Ritchie, A. C., & Warrick, J. A. (2023). The future of coastal monitoring through satellite remote sensing. *Cambridge Prisms: Coastal Futures*, *1*, e10. [Crossref]

Wang, D., Zhang, J., Du, B., Tao, D., & Zhang, L. (2023). *Scaling-up Remote Sensing Segmentation Dataset with Segment Anything Model*. http://arxiv.org/abs/2305.02034

Wang, S., Liu, Y., Feng, Y., & Lei, Z. (2021). To move or stay? A cellular automata model to predict urban growth in coastal regions amidst rising sea levels. *International Journal of Digital Earth*, *14*(9), 1213–1235. [Crossref]

Wdowinski, S., Oliver-Cabrera, T., & Fiaschi, S. (2020). Land subsidence contribution to coastal flooding hazard in southeast Florida. *Proceedings of the International Association of Hydrological Sciences*, *382*, 207–211. [Crossref]

Wojtowicz-Jankowska, D., & Bou Kalfouni, B. (2022). A Vision of Sustainable Design Concepts for Upgrading Vulnerable Coastal Areas in Light of Climate Change Impacts: A Case Study from Beirut, Lebanon. *Sustainability*, *14*(7), 3986. [Crossref]

Woodcock, C. E., Loveland, T. R., Herold, M., & Bauer, M. E. (2020). Transitioning from change detection to monitoring with remote sensing: A paradigm shift. *Remote Sensing of Environment*, *238*, 111558. [Crossref]

Xu, H. (2006). Modification of normalised difference water index (NDWI) to enhance open water features in remotely sensed imagery. *International Journal of Remote Sensing*, *27*(14), 3025–3033. [Crossref]

Yadav, S., Sahu, R. K., & Prasad, S. (2022). Land Cover Cloud Analytics: from Global Services to Regional Insights. *International Journal of Geoinformatics*, 1285–1298. [Crossref]

Zaki, A., Buchori, I., Sejati, A. W., & Liu, Y. (2022). An object-based image analysis in QGIS for image classification and assessment of coastal spatial planning. *The Egyptian Journal of Remote Sensing and Space Science*, *25*(2), 349–359. [Crossref]

Zaki, A., Buchori, I., Pangi, P., Sejati, A. W., & Liu, Y. (2023). Google Earth Engine for improved spatial planning in agricultural and forested lands: A method for projecting future ecological quality. *Remote Sensing Applications: Society and Environment*, *32*, 101078. [Crossref]

Zhang, C., & Li, X. (2022). Land Use and Land Cover Mapping in the Era of Big Data. *Land*, *11*(10), 1692. [Crossref]

Zhang, J., Zhou, Z., Mai, G., Mu, L., Hu, M., & Li, S. (2023). *Text2Seg: Remote Sensing Image Semantic Segmentation via Text-Guided Visual Foundation Models*. http://arxiv.org/abs/2304.10597

Zhang, S. (2020). Application of Remote Sensing Information Technology and Geographic Information System in Land Dynamic Monitoring. *International Journal of Geology*, *5*(1). [Crossref]

Zhang, X., & Pan, J. (2021). Spatiotemporal Pattern and Driving Factors of Urban Sprawl in China. *Land*, *10*(11), 1275. [Crossref]